On a New Nonlinear Reduced-Order Model for Capturing Internal Resonances in Intentionally Mistuned Cyclic Structures

Samuel Quaegebeur, Benjamin Chouvion, Fabrice Thouverez, Loic Berthe

ON A NEW NONLINEAR REDUCED-ORDER MODEL FOR CAPTURING INTERNAL RESONANCES IN INTENTIONALLY MISTUNED CYCLIC STRUCTURES

Samuel Quaegebeur,[1,2,*], Benjamin Chouvion[1], Fabrice Thouverez[1] and Loïc Berthe[2]

[1]École Centrale de Lyon, Laboratoire de Tribologie et Dynamique des Systèmes, UMR CNRS 5513, 36 avenue Guy de Collongue, Écully, 69134, France
[2]Safran Helicopters Engines 64511 Bordes France

ABSTRACT

Cyclic structures such as turbomachinery present material and geometrical variations between sectors. These discrepancies are called mistuning and break the cyclic symmetry of the structure. Computing the forced response of mistuned cyclic structures is thus a numerical challenge. The Component Nonlinear Complex Mode Synthesis (CNCMS) is one of the few nonlinear reduced-order model formulations that allow to compute the nonlinear response of tuned and mistuned structures. It has been validated successfully for friction problems. However, in the presence of geometric nonlinearities, internal resonances may arise and they cannot be captured correctly with the CNCMS method. The purpose of this work is therefore to present a new methodology for developing a nonlinear reduced-order model that can successfully capture internal resonances for tuned and mistuned structures. This method, called Component Mode Synthesis with Nonlinear Re-evaluation (CMSNR), is based on a variation of the CNCMS approach. The final modal synthesis uses a multi-harmonic procedure and a re-evaluation of the nonlinear forces on each sector independently. The performance and limitations of the proposed approach are assessed using a simplified example of a blisk subject to polynomial nonlinearities. Different internal resonances are exhibited and studied depending on the type of excitation force and on the level of mistuning.

Keywords: Reduced-order models, Mistuning, Polynomial nonlinearities, Internal resonance, Harmonic Balance Method

NOMENCLATURE

$\mathbf{M}$, $\mathbf{C}$, $\mathbf{K}$	Mass, damping and stiffness matrices
$\mathbf{u}$	Vector of nodal displacements
$\mathbf{I}$, $\mathbf{0}$	Identity matrix, zero matrix
$\mathbf{\Psi}$	Matrix of static mode shapes
$\mathbf{\Phi}$	Matrix of normal nonlinear mode with fixed cyclic boundaries
$\mathbf{q}$	Vector of generalized coordinates
$\mathbf{D}_{ft}$, $\mathbf{D}_{tf}$	Matrices for the Alternating Frequency Time procedure
$\mathbf{R}$	Reduction matrix
$\mathbf{Z}$	Dynamic stiffness matrix
$\mathbf{f}_{\text{nl}}$	Vector of nonlinear forces
$\mathbf{f}_{\text{ext}}$	Vector of external forces
c.c	Complex conjugates term
$\mathbf{c}$	Vector of harmonic coefficients
ω	Excitation frequency
$\mathbf{e}$	Exponential basis
$\otimes$	Kronecker product
n	Index of the nonlinear mode
k	Index of the harmonic
j	Index of the sector
i	Subscript to denote internal degrees of freedom
b	Subscript to denote boundary degrees of freedom
N_{h}	Number of harmonics
DOF	Acronym for degree of freedom
HBM	Acronym for harmonic balance method
NNM	Acronym for normal nonlinear mode
ROM	Acronym for reduced-order model
CNCMS	Acronym for complex nonlinear component mode synthesis
CNCNR	Acronym for component mode synthesis with nonlinear re-evaluation
AFT	Acronym for alternating frequency time

1. INTRODUCTION

The efficiency of airplanes has become one of the most challenging problems in aircraft companies. Turbomachinery engineers strive to reduce fuel consumption. To achieve this, the bypass ratio of turboengines is getting larger, leading to more pronounced large displacements for blades. To account for these nonlinear effects, the equations of motion of blisks have been updated with quadratic and cubic polynomial nonlinear forces that can be evaluated with a specific procedure [1]. Large displacement nonlinearities lead to complex nonlinear behavior such as internal resonances (transfer of energy between different modes)

*Corresponding author: samuel.quaegebeur@ec-lyon.fr

and bifurcation points. A bifurcation analysis [2] using specific algorithms [3] can then be used to analyze the properties of these points and reach multiple solutions. Such an analysis has been performed on large finite element models (FEM) [4] as well as on cyclic structures [5]. For large systems, reduced-order modeling (ROM) procedures are usually employed to decrease the size of the problem. The Craig-Bampton procedure [6] is widely used in mechanical engineering and reduces the number of linear degrees of freedom (DOFs). It employs a reduction matrix based on a subset of linear modes with fixed boundaries and static modes. This method has provided excellent results for linear problems. For tuned cyclic structures, symmetry properties [7] are used in parallel with a ROM procedure to express the problem in terms of cyclic components and thus to further reduce the number of unknowns. However the presence of mistuning breaks the cyclic symmetry of the structure and one generally loses the possibility to use cyclic components.

The concept of mistuning is defined as the variation in stiffness and in mass, between the sectors of a cyclic structure. A thorough review can be found in [8] and interesting vibratory behavior such as localization has been exhibited [9]. Random mistuning corresponds to small variations that can be due to fabrication discrepancies, for instance. These small variations may have a large effect on the displacement of the structure. Intentional mistuning (large but controlled variation between the sectors) is introduced in the system to lower the variation of displacement within the structure [10] and thus counter the effect of random mistuning. Moreover, intentional mistuning may be introduced for better stability against flutter [8, 11, 12]. Many numerical methods have been developed to efficiently take into account mistuning effects. The Component Mode Mistuning method (CMM) [13] is one of the most frequently used approaches and relies on the properties of the Craig-Bampton procedure [6]. It decomposes the problem into its cyclic and mistuned components and thus enables taking into account different kinds of mistuning.

When the system is subject to nonlinearities such as friction or large displacements, developing a ROM that offers both a correct description of the nonlinear phenomena and a significant gain in computation time (via an effective reduction of nonlinear DOFs) represents a genuine challenge. Different reduction methodologies for nonlinear problems exist. In the specific case of frictional effects, one could refer, for instance, to the recent work of Petrov [14], Mitra et al. [15], Pourkiaee and Zucca [16] who combined a Craig-Bampton approach with load interfaces modeshapes to reduce nonlinear mistuned system with shrouds, and to the review provided in [17]. Based on the work of Rosenberg [18], Szemplinska [19] developed the single-nonlinear-resonant-mode method. This approach is a synthesis of a forced response that utilizes a dominant nonlinear mode. Since only one mode is considered dominant, the method cannot handle internal resonances. This procedure was first applied to geometrical nonlinearities before being adapted to friction nonlinearities [20, 21]. Other reduction methods based on modal derivatives [1, 22] have been proposed for geometrical nonlinearities. Recently, Joannin et al. [23] developed the Component Nonlinear Complex Mode Synthesis (CNCMS) method. This methodology results in a very compact nonlinear ROM which was first applied to a one-dimensional simplified blisk with friction effects modeled as regularized Coulomb's law [23]. It was then successfully applied to a three-dimensional FEM blisk with intentional and random mistuning [24] and a DLFT [25] algorithm was employed to model the friction nonlinearity. The method yielded promising results in the specific case of friction nonlinearities, but is expected to lack physical representation if internal resonances are present since the nonlinear forces are substituted at the synthesis stage.

The purpose of this paper is to adapt the CNCMS method in order to offer a new ROM that can handle geometrical nonlinearities in the presence of internal resonances for both tuned and mistuned systems. This new method, called Component Mode Synthesis with Nonlinear Re-evaluation (CMSNR), creates a ROM similar to the CNCMS approach, but employs multi-harmonic modal synthesis with a re-evaluation of the nonlinear forces. This new approach is presented in Section 2. The modifications made to the CNCMS method to capture internal resonances are highlighted. Section 3 focuses on the validation of the method and its application to a simplified blisk with different types of excitation.

2. NUMERICAL PROCEDURE

In this section, the reference solution for the full-size model is presented first. An explanation of the numerical tools used throughout the entire article is included. The fundamentals of the CNCMS approach [23] are then discussed before explaining the new methodology.

2.1 Reference solution for the full-sized model

Consider a cyclic structure as depicted in Figure 1. The structure is composed of N sectors which can be different from one another due to mistuning.

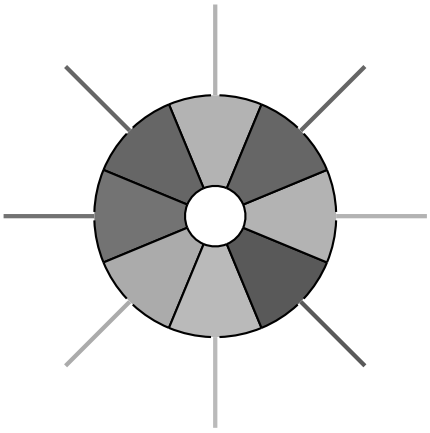

FIGURE 1: REPRESENTATION OF A CYCLIC STRUCTURE COMPOSED OF EIGHT SECTORS. THESE SECTORS ARE NOT NECESSARILY IDENTICAL.

The equation of motion of the entire structure writes

$$\mathbf{M}_\mathrm{f}\ddot{\mathbf{u}}\left(t\right)+\mathbf{C}_\mathrm{f}\dot{\mathbf{u}}\left(t\right)+\mathbf{K}_\mathrm{f}\mathbf{u}\left(t\right)+\mathbf{f}_{\mathrm{nl,f}}\left(\mathbf{u}\right)=\mathbf{f}_{\mathrm{ext,f}}, \tag{1}$$

where $\mathbf{M}_\mathrm{f}$, $\mathbf{C}_\mathrm{f}$ and $\mathbf{K}_\mathrm{f}$ denote the mass, structural and aerodynamical damping and linear stiffness matrices of the full structure.

The quantities $\mathbf{u}$, $\mathbf{f}_{\mathrm{nl,f}}$ and $\mathbf{f}_{\mathrm{ext,f}}$ are the displacement, the nonlinear forces and the external excitation forces. In this paper, geometrical nonlinearities are considered. These can be formulated as a vector of polynomial forces, written with a quadratic and cubic tensors ($\mathbf{K}_{jk}$ and $\mathbf{K}_{jkl}$) [26] such that

$$\mathbf{f}_{\mathrm{nl}} = \sum_j \sum_k \mathbf{K}_{jk}\mathbf{u}_j\mathbf{u}_k + \sum_j \sum_k \sum_l \mathbf{K}_{jkl}\mathbf{u}_j\mathbf{u}_k\mathbf{u}_l. \tag{2}$$

We use the Harmonic Balance Method (HBM) as a reference solution [27] to solve the system (1). The periodic steady state solution of the problem is sought as a Fourier series,

$$\mathbf{u}(t) = \frac{1}{2}\sum_{k=0}^{N_{\mathrm{h}}} \left(\mathbf{c}_k \mathrm{e}^{\mathrm{i}k\omega t}\right) + \mathrm{c.c}, \tag{3}$$

where $(\mathbf{c}_k)_{k\in[\![0,N_{\mathrm{h}}]\!]}$ are the Fourier coefficients, N_{h} is the maximum number of harmonics retained, ω is the excitation frequency and c.c denotes the complex conjugate terms.

After substituting (3) into (1), the system is projected (in a similar way to a Galerkin projection) along the basis $\left(\mathrm{e}_k = \mathrm{e}^{\mathrm{i}k\omega t}\right)_{k\in[\![0,N_{\mathrm{h}}]\!]}$. The scalar product employed is the Hermitian inner product,

$$\langle f, g\rangle = \frac{\omega}{\pi}\int_0^T f(t)\,\bar{g}(t)\,\mathrm{d}t, \tag{4}$$

where $\bar{g}$ denotes the complex conjugate of g.

The final algebraic system obtained after projection can then be written as:

$$\mathbf{Z}_k\mathbf{c}_k + \langle \mathbf{f}_{\mathrm{nl,f}}(\mathbf{u}), \mathrm{e}_k\rangle = \langle \mathbf{f}_{\mathrm{ext,f}}, \mathrm{e}_k\rangle \ \forall k \in [\![0, N_{\mathrm{h}}]\!], \tag{5}$$

where $\mathbf{Z}_k = -(k\omega)^2\mathbf{M}_{\mathrm{f}} + \mathrm{i}\,k\omega\mathbf{C}_{\mathrm{f}} + \mathbf{K}$ is the dynamic stiffness matrix. The nonlinear term $\langle \mathbf{f}_{\mathrm{nl,f}}(\mathbf{u}), \mathrm{e}_k\rangle$ is evaluated with the AFT procedure [28]. In the AFT procedure, the Fourier coefficients of the displacements are first transformed into time displacements $\mathbf{u}$ for a discretized time period using the inverse discrete Fourier transfer matrix, the nonlinear forces are then evaluated in the time domain before being projected back to the frequency domain with the discrete Fourier transfer matrix. This method has shown excellent results providing that the time discretization is sufficiently small.

For a finite element model of a full-sized industrial blisk, the system (5) is too large to be solved, and it is necessary to develop a ROM of the system. Among the different methods cited in the introduction, our approach is to propose a new method based on the CNCMS.

2.2 Brief description of the CNCMS procedure

The complete CNCMS method is composed of three distinct reduction stages [24] which are illustrated in Figure 2. First, a substructuring approach is used to decompose and reduce the system into N sectors to which a standard Craig-Bampton reduction is applied (see Figure 2a): the master DOFs are composed of the cyclic boundary DOFs $\left[\mathbf{u}_{j,\mathrm{b}}, \mathbf{u}_{j+1,\mathrm{b}}\right]$ and the nonlinear DOFs ($\mathbf{u}_{j,\mathrm{nl}}$). The linear DOFs ($\mathbf{u}_{j,\mathrm{lin}}$) are reduced into $\boldsymbol{\xi}$ linear generalized coordinates Next, a nonlinear Craig-Bampton procedure, depicted in Figure 2b, is performed (for each kind of intentional mistuned sector): a complex nonlinear normal mode [20] (these modes include the friction damping effects) with fixed-boundaries (a zero displacement is imposed on the cyclic boundary DOFs) and several harmonics are computed. These NNMs (similar to the linear eigenvector for a classical Craig-Bampton procedure) are supplemented with the classical static mode shapes (obtained by applying a unit displacement for each cyclic boundary DOF). The final step consists in assembling the different nonlinear superelements and employs interface modes [29] to reduce the cyclic boundary DOFs (see Figure 2c). These three successive steps give a compact nonlinear ROM. The frequency forced response of the ROM is obtained with the HBM procedure with only one harmonic. Moreover, the projection of the nonlinear forces on the Fourier basis are substituted by the complex nonlinear mode computed in the second step of the reduction procedure, performed in [21].

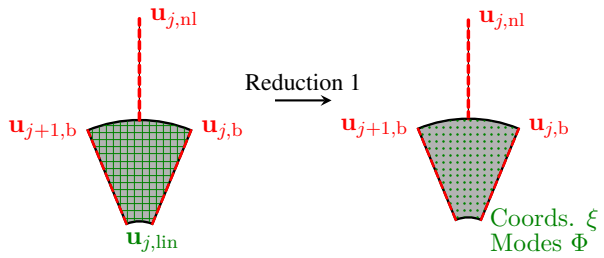

(a) Reduction 1: Linear Craig-Bampton

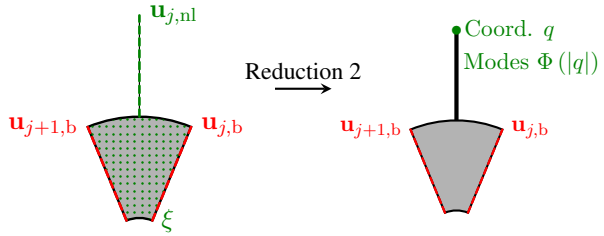

(b) Reduction 2: Noninear Craig-Bampton

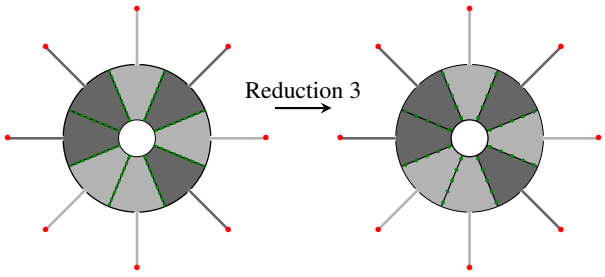

(c) Reduction 3: Interface modes

FIGURE 2: REDUCTION PROCEDURE FOR THE CNCMS AND CMSNR PROCEDURES.

2.3 Presentation of the CMSNR method

The CMSNR method has many features similar to the CNCMS. It follows the three steps presented above. The main difference is in the synthesis procedure in which the CMSNR

employs the HBM with several harmonics and a re-evaluation of the nonlinear forces (it will be detailed in Section 2.3.2). In order to validate the new approach, this article considers a lumped mass model for which there is no need to apply either the first Craig-Bampton linear reduction step or the interface modes in the final stage. For these reasons, only the developments associated with the second stage of reduction, the assembly and the synthesis of the system will be presented in this paper. Note that it is relatively straightforward to implement the first and third stages of the CNCMS method in the framework of the approach proposed.

2.3.1 Details on the second stage of reduction. This section presents the second stage of reduction which is similar in both the CNCMS and CMSNR methods. Let N be the total number of sectors composing the system (illustrated in Figure 1). These N sectors are separated in M groups of intentional mistuned sectors. The sectors are all identical within a given group (in the example of Figure 2, $N = 8$ and $M = 2$). The cyclic boundary is assumed to be free of nonlinear forces.

At the end the first stage of reduction (see Figure 2a), the displacement of sector j is decomposed into internal DOFs $\mathbf{u}_{j,\mathrm{i}} = \left[\mathbf{u}_{j,\mathrm{nl}}, \xi\right]$ and cyclic boundary DOFs (subscript cb) $\mathbf{u}_{j,\mathrm{cb}} = \left[\mathbf{u}_{j,\mathrm{b}}, \mathbf{u}_{j+1,\mathrm{b}}\right]$. The second stage of reduction keeps the cyclic boundary DOFs as master DOFs whereas the internal DOFs are reduced with the nonlinear Craig-Bampton procedure:

$$\begin{bmatrix} \mathbf{u}_{j,\mathrm{i}}(t) \\ \mathbf{u}_{j,\mathrm{cb}}(t) \end{bmatrix} = \underbrace{\begin{bmatrix} \mathbf{\Phi}_{j,1}\left(\left|\mathbf{q}_j\right|\right) & \mathbf{\Psi}_j \\ \mathbf{0} & \mathbf{I} \end{bmatrix}}_{\mathbf{R}_j\left(\left|\mathbf{q}_j\right|\right)} \begin{bmatrix} \mathbf{q}_j(t) \\ \mathbf{u}_{j,\mathrm{cb}}(t) \end{bmatrix}, \tag{6}$$

with $\mathbf{I}$ the identity matrix. $\mathbf{\Phi}_{j,1}$ and $\mathbf{q}_j$ are respectively the matrix composed of the NNMs (whose computation is explained next) and the generalized coordinates. $\mathbf{\Psi}_j$ is the matrix of the static mode shapes, obtained by applying a unit displacement for each master DOF and ensures deformation compatibility between the different sectors. It is calculated with

$$\mathbf{\Psi}_j = -\mathbf{K}_{j,\mathrm{ii}}^{-1}\mathbf{K}_{j,\mathrm{ib}}, \tag{7}$$

where $\mathbf{K}_{j,\mathrm{ii}}$ and $\mathbf{K}_{j,\mathrm{ib}}$ denote partitions (internal-internal and internal-cyclic boundary) of the stiffness matrix of sector j (a similar notation will be used for the mass and dynamic stiffness matrices later on).

The NNMs for sector j are obtained by imposing a zero displacement at the cyclic boundary DOFs and searching for the periodic solution of the following equation

$$\mathbf{M}_{j,\mathrm{ii}}\ddot{\mathbf{u}}_{j,\mathrm{i}}(t) + \mathbf{K}_{j,\mathrm{ii}}\mathbf{u}_{j,\mathrm{i}}(t) + \mathbf{f}_{\mathrm{nl},j} = \mathbf{0}. \tag{8}$$

Employing the HBM on the previous equation gives:

$$\mathbf{Z}_{j,k,\mathrm{ii}}\mathbf{c}_{j,k,\mathrm{i}} + \langle \mathbf{f}_{\mathrm{nl},j}, \mathrm{e}_k \rangle = \mathbf{0}, \ \forall k \in [\![0, N_\mathrm{h}]\!], \tag{9}$$

where $\mathbf{c}_{j,k,\mathrm{i}}$ denotes the $k-$th harmonic of the interior DOFs of sector j. The NNM n is obtained by solving (9) with a pseudo-arclength procedure [30] initialized on the linear mode n. As explained in [18], the displacement of all the DOFs is controlled by a single DOF (also called control coordinate $q_{n,j}$ for a sector j and a NNM n). The harmonics $\mathbf{c}_{j,k,\mathrm{i}}$ (that may be non-similar, i.e. their shapes vary with the amplitude) and the pulsation ω directly depend on the control coordinate. The nonlinear mode $\mathbf{\Phi}_{n,j,k}$ used for the reduction is defined as equal to the harmonics $\mathbf{c}_{j,k,\mathrm{i}}$ normalized by the control coordinate. In Section 3, the control coordinate is taken as equal to the first harmonic of one of the DOFs.

The NNMs are computed with one harmonic ($N_\mathrm{h} = 1$) simply to avoid problems in the synthesis procedure in which a bijective property must be ensured between the curvilinear abscissa and the control coordinate. For a single harmonic the amplitude of the system will increase with the curvilinear abscissa (increase of energy). However, with several harmonics, additional branches (tongues) may be obtained due to internal resonances [27] and thus lead to the loss of the bijective property. The authors have chosen to remove these singularities by taking only one harmonic, although a particular postprocessing of the multi-harmonics NNM is also possible.

The system dynamics of the sector is controlled by the different NNMs, as underlined in (6), where $\mathbf{\Phi}_{j,1} = \left[\mathbf{\Phi}_{1,j,1}, ..., \mathbf{\Phi}_{n,j,1}\right]$. Similarly, the control coordinate $\mathbf{q}_j$ is composed of the different control coordinates $\left[q_{1,j}, ..., q_{n,j}\right]$ for the different NNMs. The reduction basis $\mathbf{R}_j$ is a function of the amplitude of the control coordinates $\left(\mathbf{q}_j\right)$. However, to simplify the notation, the dependency in $\mathbf{q}$ on the reduction matrix will be omitted later. Note that $\mathbf{R}_j$ must be computed only for the M types of sector.

2.3.2 Assembly and synthesis procedure. Applying the reduction procedure to the equation of motion (1) for a single sector j, gives

$$\mathbf{R}_j^T\mathbf{M}_j\mathbf{R}_j \begin{bmatrix} \ddot{\mathbf{q}}_j(t) \\ \ddot{\mathbf{u}}_{j,\mathrm{cb}}(t) \end{bmatrix} + \mathbf{R}_j^T\mathbf{C}_j\mathbf{R}_j \begin{bmatrix} \dot{\mathbf{q}}_j(t) \\ \dot{\mathbf{u}}_{j,\mathrm{cb}}(t) \end{bmatrix} + \mathbf{R}_j^T\mathbf{K}_j\mathbf{R}_j \begin{bmatrix} \mathbf{q}_j(t) \\ \mathbf{u}_{j,\mathrm{cb}}(t) \end{bmatrix} + \mathbf{R}_j^T\mathbf{f}_{\mathrm{nl},j} = \mathbf{R}_j^T\mathbf{f}_{\mathrm{ext},j} \tag{10}$$

The external forces $\mathbf{f}_{\mathrm{ext},j}$ are assumed to be periodic with a fundamental frequency ω. In practical applications, they may be due to aerodynamical loading. More complex excitations may be considered such as multiple excitation frequencies or aerocoupling effect incorporated directly in the nonlinear forces. In our case, the steady-state physical displacements (and thus the generalized coordinates) are assumed to be periodic, with the same frequency as the excitation force. The HBM is thus performed on the generalized coordinates and the cyclic boundary DOFs. They are sought after as

$$\begin{bmatrix} \mathbf{q}_j(t) \\ \mathbf{u}_{j,\mathrm{cb}}(t) \end{bmatrix} = \frac{1}{2}\left(\begin{bmatrix} \sum_{k=0}^{N_\mathrm{h}} \mathbf{p}_{j,k}\mathrm{e}^{\mathrm{i}k\omega t} \\ \sum_{k=0}^{N_\mathrm{h}} \mathbf{c}_{j,k,\mathrm{b}}\mathrm{e}^{\mathrm{i}k\omega t} \end{bmatrix} + \mathrm{c.c}\right), \tag{11}$$

where $\mathbf{p}_j = \left[\mathbf{p}_{j,0}, ..., \mathbf{p}_{j,N_\mathrm{h}}\right]^T$ correspond to the vectors of the Fourier coefficients of $\mathbf{q}_j$. Projecting (10) onto the $(\mathrm{e}_k)_{k\in[\![0,N_\mathrm{h}]\!]}$ basis gives

$$\mathbf{R}_j^T\mathbf{Z}_{k,j}\mathbf{R}_j \begin{bmatrix} \mathbf{p}_{j,k} \\ \mathbf{c}_{j,k,\mathrm{b}} \end{bmatrix} + \langle \mathbf{R}_j^T\mathbf{f}_{\mathrm{nl},j}, \mathrm{e}_k \rangle = \langle \mathbf{R}_j^T\mathbf{f}_{\mathrm{ext},j}, \mathrm{e}_k \rangle \ \forall k \in [\![0, N_\mathrm{h}]\!]. \tag{12}$$

The CNCMS method substitutes the projected nonlinear forces, $\langle \mathbf{R}_j^T \mathbf{f}_{\mathrm{nl},j}, e_k \rangle$, by the NNM computed in (9). As explained in [21], this substitution implies an approximation as the NNMs are not computed at the excitation frequency. Furthermore, the substitution results in a decoupled set of equations: each harmonic is independent. In the case of friction nonlinearities, this approximation has shown excellent results [24]. However, in the case of geometrical nonlinearities where internal resonances may occur, this simplification prevents recovering the full behavior. Therefore, we propose not to make this assumption but to re-evaluate the nonlinear forces via the AFT procedure [28]. This computation is done for each sector separately and allows possible couplings between different NNMs. The nonlinear forces are computed in the time domain using the displacements of the internal DOFs obtained via (6) and (11).

The system of equations (12) is then assembled for each sector along their cyclic boundary DOFs and this gives:

$$\mathbf{Z}_{r,k} \begin{bmatrix} \mathbf{p}_k \\ \mathbf{c}_{k,\mathrm{b}} \end{bmatrix} + \mathbf{f}_{\mathrm{nl},r,k} = \mathbf{f}_{\mathrm{ext},r,k} \;\; \forall k \in [\![0, N_\mathrm{h}]\!], \tag{13}$$

where $\mathbf{Z}_{r,k}$ is the complete reduced dynamic stiffness matrix and depends on $|\mathbf{q}|$, $\mathbf{p}_k$ denotes the generalized coordinates of the entire structure for all the NNMs for the $k-$th harmonic, $\mathbf{c}_{k,\mathrm{b}}$ corresponds to the $k-$th harmonic of the cyclic boundary DOFs. The vectors $\mathbf{f}_{\mathrm{nl},r,k}$ and $\mathbf{f}_{\mathrm{ext},r,k}$ are the reduced nonlinear forces and reduced external forces, respectively, projected on the $k-$th harmonic.

The system (13) is square and can be solved using a Newton-Raphson procedure. Since the reduction basis relies on the computation of the NNMs for a discretized number of points, the algorithm employs a linear interpolation of the NNM, a priori calculated along the control coordinate. Sufficiently refined NNMs are thus required for accurate results. To ensure fast-computation, the Jacobian of the system (13) may be provided. Joannin et al. gave the formulation of this quantity for the CNCMS [23]. However, the CMSNR re-evaluates the nonlinear forces and thus the Jacobian is different compared to the CNCMS method, see details in Appendix A.

3. NUMERICAL RESULTS

3.1 Presentation of the test case

The concept of the CNCMS approach was successfully tested on a 3D FEM [24]. Considering such an example with geometrical nonlinearities first requires evaluating the nonlinear stiffness tensors (quadratic and cubic terms) with appropriate methods such as that explained in [1]. This is beyond the scope of the current work and we focus on validating and assessing the CMSNR with regard to a full resolution of the system (not conceivable for a 3D FEM). Therefore, the choice was made to work on a phenomenological model of a blisk containing a single nonlinear DOF per sector. The cyclic structure considered is represented in Figure 3. For this test case, the full system (5) can be solved in a reasonable amount of time and the associated results will act as the reference solution. Tuned and mistuned systems are studied.

The tuned system is composed of 24 identical sectors noted A. For this sector A, the mass values are chosen to be representative of a real blisk mass distribution. Spring stiffness values are calculated such that the first bending mode family matches that of a real blisk. A modal damping of 0.1% is used, which is representative of a classical structural damping [31].

The mistuned system is composed of 24 sectors with the classical alternate mistuning pattern [A ,B, A, B,...] (this pattern is typical to eliminate the flutter problem [32]). Sector B differs from sector A in only spring stiffnesses that are varied in order to obtain a 5% shift of the first eigenfrequency. All the numerical values used are reported in Tables 1 and 2. In addition to this detuning, a perturbation (random mistuning) is applied to the spring stiffness value between the tip and middle masses. It is defined as

$$k_m = k_t \, (1 + \varepsilon \xi) \, , \tag{14}$$

where k_m and k_t represent the mistuned and tuned stiffness values, and ξ is taken randomly in the uniform continuous range $[-0.01, 0.01]$ (1% of variation). Those values are provided in Appendix B. The coefficient ε will be chosen between 0 and 1 in order to assess the impact of the random mistuning on the internal resonance.

A similar tuned model was used in [33] with friction nonlinearities. The nonlinear effects considered in this study correspond to a symmetric large displacement of the tip of the blade. In pronounced large displacements of new blade designs (larger blades with a relative thinner section), both quadratic and cubic terms appear as nonlinear forces. Although the new method can handle both terms, the nonlinearity of the test case is modeled with a cubic nonlinear stiffness only, which is the dominant term in the case of a symmetrical dynamic behavior. This cubic stiffness k_{nl}, taken equal to 2×10^9 N m^{-3}, is placed in parallel to a linear spring stiffness. An external force is applied to the tip mass (m_1). The excitation follows either a traveling or a standing wave pattern along a specific nodal diameter. The frequency responses in the results section illustrate the displacement of the tip mass.

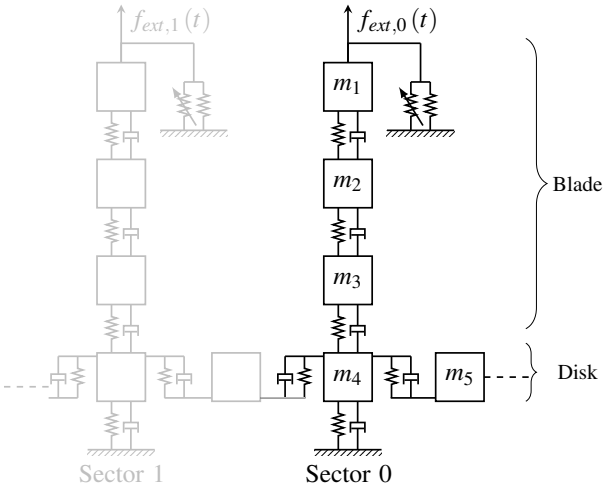

FIGURE 3: REPRESENTATION OF THE TEST CASE

In the following section, the CMSNR is employed and compared to both the full HBM resolution presented in Section 2.1 and the CNCMS method. The purpose is to verify that the ROM enables capturing complex phenomena such as internal resonances.

m_1	m_2	m_3	m_4	m_5
0.2	0.3	0.4	1.2	1.2

TABLE 1: NUMERICAL VALUES FOR THE DIFFERENT MASSES, IN kg

Parts	k $(10^6\,\mathrm{N\,m^{-1}})$ Sector A	Sector B	c $(\mathrm{N\,s\,m^{-1}})$
Tip/Ground	0.1	0.1	0
Tip/Middle	2	1.8	1.3
Middle/Foot	1	0.9	0.7
Foot/Disk	40	40	26.7
Disk/Boundary	50	50	33.3
Disk/Ground	0.6	0.6	0.4

TABLE 2: NUMERICAL VALUES FOR THE DIFFERENT SPRING STIFFNESSES AND DAMPERS

Several explanations will be provided but a full analysis of the nonlinear interaction phenomena can be found in [34, 35].

3.2 Tuned system

We first consider a perfectly tuned system composed of 24 sectors (of type A). Figure 4 presents its natural frequencies for each nodal diameter. This frequency/diameter graph is typical of a real blisk.

For this tuned test case, a standing wave excitation is applied. It was shown in [35] that an excitation of this kind facilitates the occurrence of internal resonances. The NNMs are computed following the procedure in Section 2.3.1 and the static mode shapes are computed with (7).

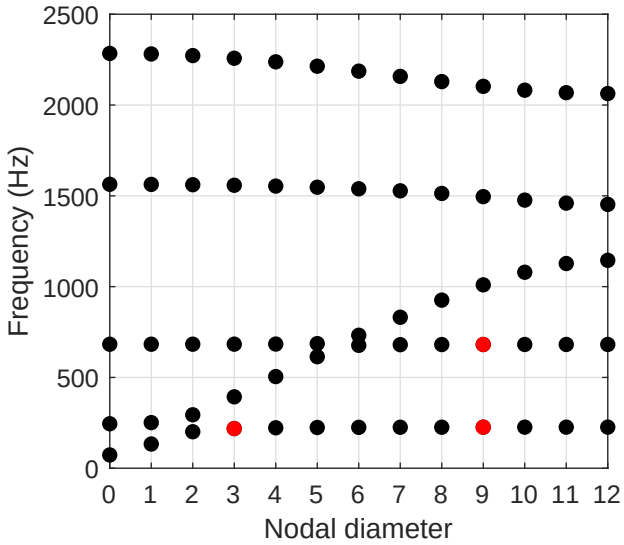

FIGURE 4: NATURAL FREQUENCIES OF EACH NODAL DIAMETER (RED CIRCLES REPRESENT THE MODES OF INTEREST FOR THE 3-9).

In each of the following simulations, four results will be compared: the reference solution explained in Section 2.1 (calculation on the full structure), the CMSNR method with only the first two NNMs, the CMSNR method with a complete reduction basis (all 4 NNMs are computed), and the CNCMS procedure (with all 4 NMMs). It must be emphasized that the latter simulations do not provide a reduction of unknowns but projects the system on a new complete nonlinear basis. Five harmonics are retained in the HBM method for the reference solution and the CMSNR. The results are evaluated for the full structure and are then projected on the cyclic components of the system [36] with:

$$\tilde{u}_p = \sum_{j=0}^{N} u_j \mathrm{e}^{\mathrm{i}j\alpha p}, \tag{15}$$

where $\tilde{u}_p$ denotes the $p-$th wave component of the deformation shape. Only the relevant components will be represented for the tuned test case. Moreover, the harmonic coefficients of the different cyclic components will also be depicted. They were calculated for the CMSNR with 4 NNMs simulations and are represented as figure insets.

Interpretations of the different simulations will be provided in Section 3.2.2, while the method's performance will be assessed in Section 3.4.

3.2.1 Forced response simulation. A 25 N standing wave excitation following a three nodal diameter pattern is applied at the tip of the blade. Figure 5 illustrates the frequency response obtained with this excitation. A coupling between the third and ninth nodal diameters is revealed.

The CMSNR method with all the NNMs (blue curve) gives the same results as the reference (green square). Taking all the NNMs in the reduction basis provides a fully converged ROM. Taking only the first two NNMs (red crosses) provides the correct trends with a slight increase in amplitude (around 226 Hz and 229 Hz) and a slight shift in frequency. This loss of accuracy for a ROM with only two NNMs is expected: the sector is composed of five DOFs and each NNM plays an important part in the global dynamic of the system. In a similar way to the usual Craig-Bampton procedure, better accuracy is obtained when more NNMs are retained in the ROM, with the drawback of longer computation time. The CNCMS does not converge towards the reference solution.

3.2.2 Interpretations. Figure 5 shows that the main component of the excited nodal diameter ($\tilde{u}_3$) is the first harmonic (as expected due to the mono-harmonic external excitation). However, the ninth nodal diameter has a non-zero component and its first and third harmonics respond. This depicts a 1:1 internal resonance as well as a 1:3 internal resonance. The external forces excite the third diameter of the structure. Due to coupling from the nonlinear forces, the ninth nodal diameter also responds (presence of terms similar to $\tilde{u}_3^3$) and thus an internal resonance occurs. Although commensurable frequencies are not mandatory [5], these internal resonances might have been predicted as $\tilde{f}_{3,1} \approx \tilde{f}_{9,1}$ and $\tilde{f}_{9,2} \approx 3\tilde{f}_{3,1}$ (see the numerical values of the frequencies in Table 3). This corroborates the results found in [35] where it was shown that combining a cubic nonlinearity with an excitation of the blisk along the third nodal diameter may result in energy exchange between the third and ninth nodal diameter.

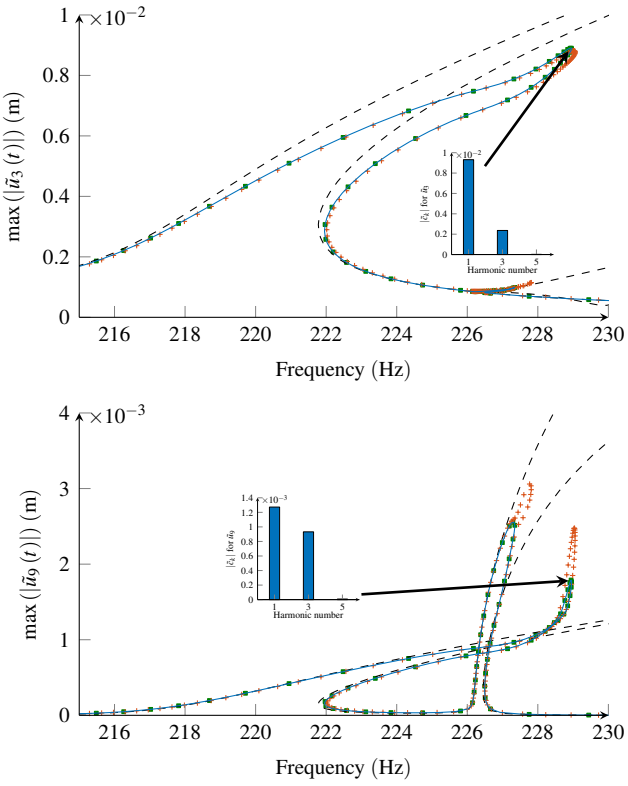

FIGURE 5: FREQUENCY RESPONSE FUNCTION PROJECTED ON THE THIRD AND NINTH NODAL DIAMETER. (■): REFERENCE SOLUTION; (+): CMSNR SOLUTION OF THE ROM WITH THE FIRST TWO NNMS; (—): CMSNR SOLUTION OF THE ROM CONTAINING ALL NNMS; (- -): CNCMS RESULTS. BOX INSETS REPRESENT THE HARMONICS OF THE RESPONSE AT RESONANT PEAKS.

	Mode 1	Mode 2	Mode 3	Mode 4	Mode 5
$\tilde{f}_3$	218.54	393.15	683.25	1558.24	2257.67
$\tilde{f}_9$	226.08	681.36	1009.82	1495.64	2102.93

TABLE 3: NATURAL FREQUENCIES FOR THE NODAL DIAMETER NUMBERED 3 AND 9, IN (Hz). THE FREQUENCIES IN COLOR CORRESPOND TO THE COLORED MODES DEPICTED IN FIGURE 4.

A sufficiently high excitation is required to obtain an internal resonance [37]. Including the effect of aero-damping is perfectly conceivable in the proposed ROM formulation. It is expected that a positive damping would lower the amplitude of the system and thus decrease the probability of the occurrence of internal resonances, whereas a negative damping (such as the flutter phenomenon) would have the opposite effect.

For this simulation, the discrepancies between the CNCMS and the reference solution justify the need for a new method capable of recovering complex phenomena occurring with geometrical nonlinearities.

3.3 Mistuned system

This section is split into two parts. The system is first intentionally mistuned (as explained in Section 3.1). The effect of random mistuning on the internal resonances of the main branch of solution is next studied. The objectives are to validate the proposed ROM on a realistically mistuned blisk and to study the effect of (intentional and random) mistuning on the nonlinear forced response of the structure.

3.3.1 Intentional mistuning. A 5 N standing wave excitation following a twelve nodal diameter pattern is used in this first simulation. Due to the pattern of the intentional mistuning, the system remains cyclic and only the zero and twelfth nodal diameter respond. The frequency response of these components is shown in Figure 6. One can observe a 1:3 internal resonance within the box inset: the twelfth nodal diameter is directly excited with a single harmonic while the zeroth diameter responds with harmonics 1 and 3.

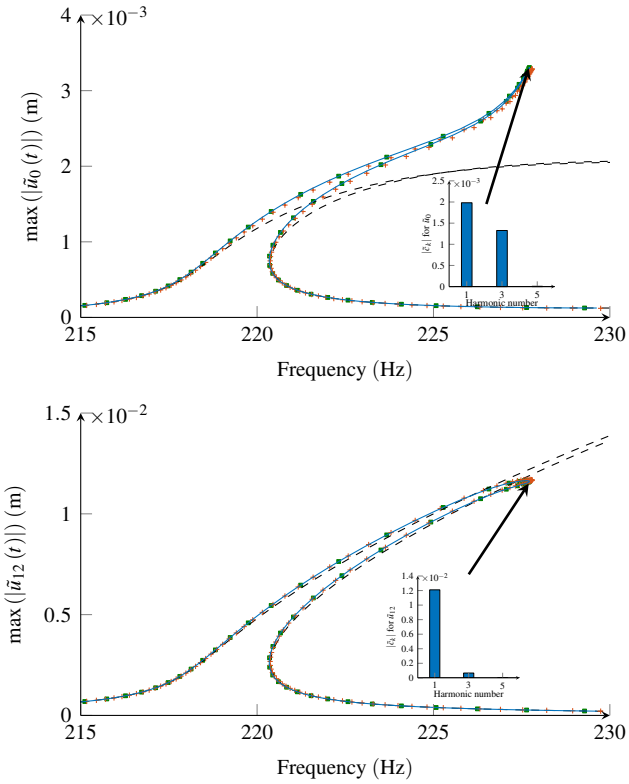

FIGURE 6: FREQUENCY RESPONSE FUNCTION FOR THE ZERO AND TWELFTH NODAL DIAMETERS. THE COLOR LINES MATCH THE DESCRIPTION PROVIDED IN FIGURE 5.

As described earlier, the full CMSNR ROM perfectly matches the reference solution, and manages to correctly describe the different resonances. It gives a slightly different amplitude for each peak if only two NNMs are retained in the reduced system. Again, the CNCMS is not able to recover the correct response amplitude.

3.3.2 Fully mistuned structure. A random mistuning (see Equation (14)) is now introduced on top of the previously intentionally mistuned system. The same excitation force is used. The purpose of this short analysis is to study the impact of random mistuning on the internal resonance illustrated in Figure 6. The reference solution is compared with the CMSNR method (with 2 NNMs). Two different methodologies are used to compute the

frequency response function. First, the classical application of the HBM procedure (with pseudo arc-length continuation) on the mistuned system is employed for $\varepsilon = 0.3$ and $\varepsilon = 1$. Next, an homotopy procedure is used to evaluate the evolution of the main branch of solution shown in Figure 6 with random mistuning. For this matter, the level of random mistuning is progressively raised (ε starts at 0 and is increased by 10^{-3} until the final value of 1). In each step, the solver is initialized on the previous solution.

Due to random mistuning, frequency splitting occurs [33] and the amplitude of all other cyclic components raises as ε increases. These components are not studied in this paper. The focus is made on the zero and twelfth cyclic components that are the main subjects of the internal resonance shown in Figure 6. Their frequency responses are illustrated in Figures 7 and 8 for $\varepsilon = 0.3$ and $\varepsilon = 1$, and for different methods of simulation.

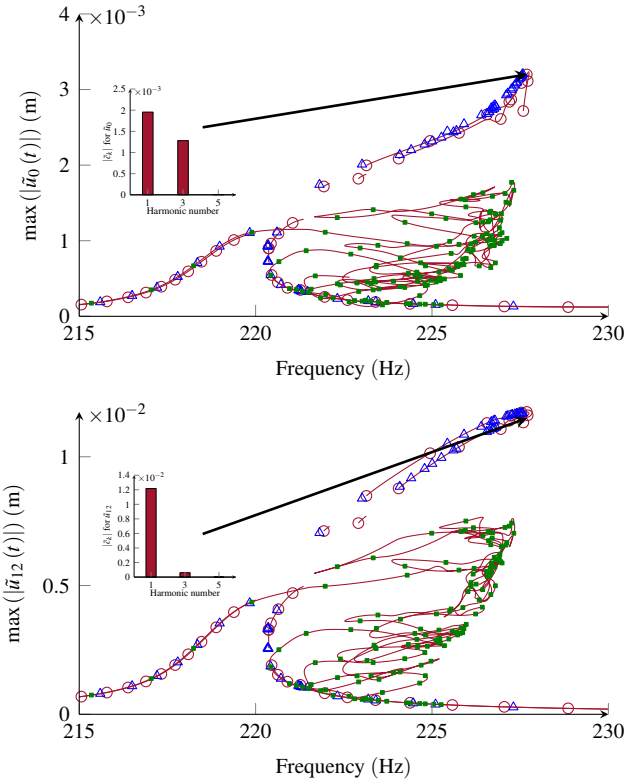

FIGURE 7: FREQUENCY RESPONSE FUNCTION FOR THE ZERO AND TWELFTH NODAL DIAMETERS WITH RANDOM MISTUNING $\varepsilon = 0.3$. (—): CMSNR WITH CONTINUATION; (-o-): CMSNR WITH HOMOTOPY; (■): REFERENCE SOLUTION WITH CONTINUATION; (△): REFERENCE SOLUTION WITH HOMOTOPY.

In both Figures, the reference solution (■) perfectly match with the CMSNR (—) results for the classical continuation procedure. Pockets of solutions [38] whose interpretation is beyond the scope this paper are obtained. The capability of the CMSNR to retrieve those solutions shows the robustness of this new methodology.

The homotopy procedure, represented with (-o-) for the CMSNR approach and (△) for the reference solution, manages to capture parts of the internal resonance of Figure 6. For $\varepsilon = 0.3$ in Figure 7, the internal resonance peak is obtained and the box

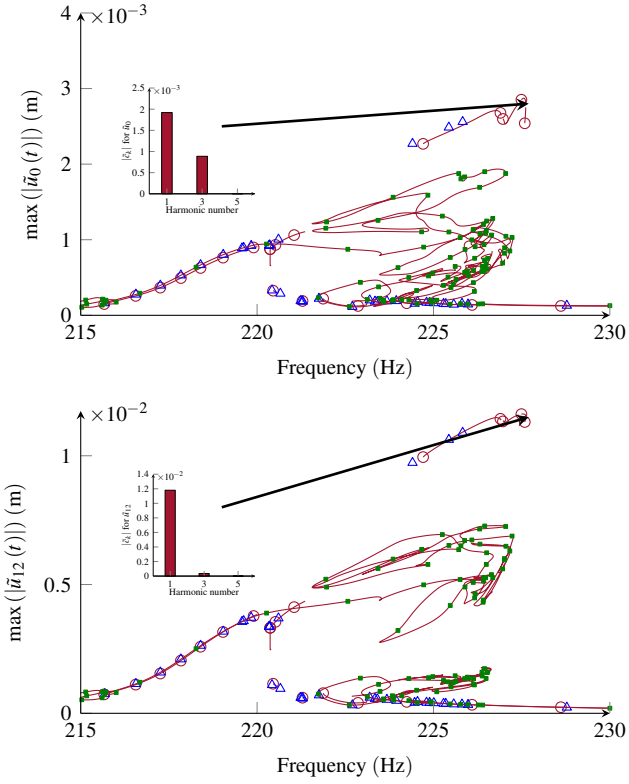

FIGURE 8: FREQUENCY RESPONSE FUNCTION FOR THE ZERO AND TWELFTH NODAL DIAMETERS WITH RANDOM MISTUNING $\varepsilon = 1$. (—): CMSNR WITH CONTINUATION; (-o-): CMSNR WITH HOMOTOPY; (■): REFERENCE SOLUTION WITH CONTINUATION; (△): REFERENCE SOLUTION WITH HOMOTOPY.

insets still depict the 1:3 internal resonance. For $\varepsilon = 1$ in Figure 8, the peak starts to disappear and the box insets reveal that the internal resonance is diminished. For both of these figures, a gap in the main branch of solution between $220 - 222$ Hz is obtained and increases with the value ε. This gap relates to the presence of pocket of solutions obtained with the continuation procedure. Overall the CMSNR results closely match the ones from the reference solution.

These first results seem to indicate that random mistuning tends to break the occurrence of internal resonance within the main branch of solutions. It may then be possible to remove these internal resonances with a specific pattern of intentionally mistuned blades. The classical pattern [A,B,A,..] is not recommended to achieve this because it still presents cyclic symmetry properties.

Further analysis should be carried out to obtain a definitive statement (for instance, a bifurcation analysis [39] and/or a detailed Floquet analysis to assess the stability of the solution). These algorithms are expected to work with the reduction procedure but are beyond the scope of the paper which focused on the validity of a new reduction approach valid even if internal resonances exist.

3.4 Computational performance of the method

Finally, the performance of the ROM is summarized in Table 4. The number of unknowns and the associated computational time are provided.

Method	Number of unknowns	Computation time (s)
Reference	360	140 / 113.9
CMSNR (2 NNMs)	216	60 / 50.8
CMSNR (4 NNMs)	360	106 / 90.4

TABLE 4: REDUCTION AND ASSESSMENT OF COMPUTING GAIN. THE COMPUTATION TIME VALUES IN THE THIRD COLUMN CORRESPOND TO THE SIMULATIONS ILLUSTRATED IN FIGURES 5/ 6 (IN THIS ORDER). THE SIMULATIONS WERE RUN ON A STANDARD COMPUTER: INTEL(R) CORE(TM) I7-7700 @ 3.6 GHZ.

The computation time of an NNM is less than 10 s and is thus relatively small compared to the synthesis procedure (note that the NNM is evaluated only once and can then be used for all the synthesis procedures whose results are shown in Figures 5 and 6). The computation time for the ROM with two NNMs is less than half the computation time of the reference. This ROM still provides good correlation, and shows the advantage of the proposed approach. Moreover, the full ROM is approximately 10% faster than the reference solution. This result may seem surprising because the number of DOFs is the same in both methods and because the ROM also requires an interpolation procedure. However, the gain in computational time is due to the assumption made in the reduced model (the nonlinear forces are computed for each sector separately) which makes the AFT procedure faster to compute than in the reference solution. In a detailed finite element model, the authors expect the gain in computation time to be even larger.

CONCLUSION

The proposed approach, namely Component Mode Synthesis with Nonlinear Reevaluation (CMSNR), is similar to the CNCMS method in the way that the ROM is composed of normal nonlinear modes, obtained for a sector with fixed boundaries and static mode shapes. Each sector is then considered as a nonlinear superelement. The nonlinear modes are computed without modal interaction. However, the synthesis in the CMSNR allows to couple together all the modes by re-evaluating the nonlinear forces on each sector separately. Modal interaction is then properly accounted for. This procedure was tested successfully on a simplified blisk. The proposed ROM showed good accuracy with a gain in computation time and was able to recover complex phenomena such as internal resonances in tuned and mistuned test cases. Moreover the ROM proposed was shown to be suitable for studying the impact of mistuning on internal resonances. The internal resonance of the main branch of solutions progressively disappeared for increasing values of random mistuning. As illustrated with different simulations, the CNCMS was not suited to capturing internal resonances and could thus lead to inappropriate conclusions.

For those interested in a realistic FEM, the new procedure can easily be supplemented with the first (usual Craig Bampton reduction) and third (use of interface modes) reductions of the CNCMS procedure. The three reduction steps would produce a nonlinear ROM for finite element models capable of capturing internal resonances at reduced computational cost. However, other challenges arise for realistic finite element models such as the evaluation of the nonlinear stiffness matrix. Some methods, like the STEP approach [26], have been proposed for this type of evaluation. Work in the future could involve using the STEP method with our reduction procedure.

In the CMSNR proposed, the choice of which NNM to consider in the reduction basis plays an important part of the reduction procedure.The NNMs initialized on the linear modes whose frequencies are commensurable or near-commensurable with the excitation frequency should be computed to capture internal resonances. Moreover, the assumption of computing the nonlinear forces separately and assembling the structure with static mode shapes assumes linearity in the cyclic boundaries which may not hold for specific structures.

ACKNOWLEDGEMENT

The authors are grateful for the financial support of Safran Helicopter Engines and the Ecole Centrale Lyon. Samuel Quaegebeur would also would like to thank Adrien Martin for his help in using the tikz software to draw the sketches.

APPENDIX A. EVALUATION OF THE JACOBIAN

The Jacobian of the system (13) is first evaluated for each sector independently before being assembled. The differentiations of the system (12) with respect to the variables $\mathbf{p}_{j,k}$ and $\mathbf{c}_{j,k,\mathrm{b}}$ are needed. Due to the dependency of the reduction basis in $\mathbf{q}$, a complete analytical Jacobian is not possible. A semi-analytical Jacobian was provided for the CNCMS procedure in [23]. Most of its steps can be re-employed for the new procedure except for the Jacobian of the nonlinear forces. The nonlinear forces are obtained via the AFT as described in Section 2.1. Therefore, the Jacobian is defined with

$$\begin{cases} \dfrac{\mathrm{d}\mathbf{f}_{\mathrm{nl},j}}{\mathrm{d}\mathbf{p}^{\mathrm{re}}_{j,k}} = \mathbf{D}_{tf}\dfrac{\mathrm{d}\mathbf{f}^{temp}_{\mathrm{nl},j}}{\mathrm{d}\mathbf{u}^{temp}_{j}}\dfrac{\mathrm{d}\mathbf{u}^{temp}_{j}}{\mathrm{d}\mathbf{p}^{\mathrm{re}}_{j,k}} & (16)\\ \dfrac{\mathrm{d}\mathbf{f}_{\mathrm{nl},j}}{\mathrm{d}\mathbf{p}^{\mathrm{im}}_{j,k}} = \mathbf{D}_{tf}\dfrac{\mathrm{d}\mathbf{f}^{temp}_{\mathrm{nl},j}}{\mathrm{d}\mathbf{u}^{temp}_{j}}\dfrac{\mathrm{d}\mathbf{u}^{temp}_{j}}{\mathrm{d}\mathbf{p}^{\mathrm{im}}_{j,k}} & (17)\\ \dfrac{\mathrm{d}\mathbf{f}_{\mathrm{nl},j}}{\mathrm{d}\mathbf{c}^{\mathrm{re}}_{j,k,\mathrm{b}}} = \mathbf{D}_{tf}\dfrac{\mathrm{d}\mathbf{f}^{temp}_{\mathrm{nl},j}}{\mathrm{d}\mathbf{u}^{temp}_{j}}\dfrac{\mathrm{d}\mathbf{u}^{temp}_{j}}{\mathrm{d}\mathbf{c}^{\mathrm{re}}_{j,k,\mathrm{b}}} & (18)\\ \dfrac{\mathrm{d}\mathbf{f}_{\mathrm{nl},j}}{\mathrm{d}\mathbf{c}^{\mathrm{im}}_{j,k,\mathrm{b}}} = \mathbf{D}_{tf}\dfrac{\mathrm{d}\mathbf{f}^{temp}_{\mathrm{nl},j}}{\mathrm{d}\mathbf{u}^{temp}_{j}}\dfrac{\mathrm{d}\mathbf{u}^{temp}_{j}}{\mathrm{d}\mathbf{c}^{\mathrm{im}}_{j,k,\mathrm{b}}}, & (19) \end{cases}$$

where the superscript "re" and "im" denote the real and imaginary part, $\mathbf{u}^{temp}_{j}$ represents the time displacement of sector j. $\mathbf{D}_{ft}$ and $\mathbf{D}_{tf}$ are respectively the direct and inverse discrete

Fourier transfer matrices. The term $\frac{\mathrm{d}\mathbf{f}_{\mathrm{nl},j}^{temp}}{\mathrm{d}\mathbf{u}_j^{temp}}$ corresponds to the differentiation of the nonlinear forces of sector j in the time domain with respect to the displacement in the time domain. The computation of this term is immediate due to the regular law governing the nonlinear forces and only the last four differentiations of the right-hand side of (16)-(19) require special attention.

The time displacements of the internal DOFs are obtained via relation (6)

$$\mathbf{u}_j^{temp} = \mathbf{D}_{ft}\left(\left(\mathbf{I}_{N_\mathrm{h}+1}\otimes\mathbf{\Phi}_{j,1}\right)\mathbf{p}_j + \left(\mathbf{I}_{N_\mathrm{h}+1}\otimes\mathbf{\Psi}_j\right)\mathbf{c}_{j,\mathrm{b}}\right) + \mathrm{c.c} \quad (20)$$

where $\otimes$ represents the Kronecker product.

The differentiation with respect to the variables $\mathbf{p}_{j,k}^{\mathrm{re}}$, $\mathbf{p}_{j,k}^{\mathrm{im}}$, $\mathbf{c}_{j,k,\mathrm{b}}^{\mathrm{re}}$ and $\mathbf{c}_{j,k,\mathrm{b}}^{\mathrm{im}}$ are given by

$$\begin{cases}
\dfrac{\mathrm{d}\mathbf{u}_j^{temp}}{\mathrm{d}\mathbf{p}_{j,k}^{\mathrm{re}}} = \mathbf{D}_{ft}\left(\left(\mathbf{I}_{N_\mathrm{h}+1}\otimes\mathbf{\Phi}_{j,1}\right) + \left(\mathbf{I}_{N_\mathrm{h}+1}\otimes\dfrac{\mathrm{d}\mathbf{\Phi}_{j,1}}{\mathrm{d}\mathbf{p}_{j,k}^{\mathrm{re}}}\right)\mathbf{p}_j\right) + \mathrm{c.c} & (21)\\
\dfrac{\mathrm{d}\mathbf{u}_j^{temp}}{\mathrm{d}\mathbf{p}_{j,k}^{\mathrm{im}}} = \mathbf{D}_{ft}\left(\left(\mathrm{i}\mathbf{I}_{N_\mathrm{h}+1}\otimes\mathbf{\Phi}_{j,1}\right) + \left(\mathbf{I}_{N_\mathrm{h}+1}\otimes\dfrac{\mathrm{d}\mathbf{\Phi}_{j,1}}{\mathrm{d}\mathbf{p}_{j,k}^{\mathrm{im}}}\right)\mathbf{p}_j\right) + \mathrm{c.c} & (22)\\
\dfrac{\mathrm{d}\mathbf{u}_j^{temp}}{\mathrm{d}\mathbf{c}_{j,k,\mathrm{b}}^{\mathrm{re}}} = \mathbf{D}_{ft}\left[\left(\mathbf{I}_{N_\mathrm{h}+1}\otimes\mathbf{\Psi}_j\right)\right] + \mathrm{c.c} & (23)\\
\dfrac{\mathrm{d}\mathbf{u}_j^{temp}}{\mathrm{d}\mathbf{c}_{j,k,\mathrm{b}}^{\mathrm{im}}} = \mathbf{D}_{ft}\left[\left(\mathrm{i}\mathbf{I}_{N_\mathrm{h}+1}\otimes\mathbf{\Psi}_j\right)\right] + \mathrm{c.c}, & (24)
\end{cases}$$

These terms are evaluated numerically and substituted into (16)-(19) to obtain the Jacobian on one sector. Each term is then assembled, along the boundary DOFs, to form the full Jacobian.

APPENDIX B. RANDOM MISTUNING VALUES

	S1	S2	S3	S4	S5	S6
ξ_1	0	−8.8	−9.2	0.4	6.4	4.5
	S7	S8	S9	S10	S11	S12
	3.2	9.5	6.0	−1.4	−8.3	−6.5
	S13	S14	S15	S16	S17	S18
	6.6	−8.8	0.5	3.1	−4.2	−9.7
	S19	S20	S21	S22	S23	S24
	−6.7	−2.6	−0.2	9.0	−8.9	−4.6

TABLE 5: RANDOM STIFFNESS VALUES $\xi(\times 10^{-3})$ FOR SECTOR S1 TO SECTOR S24.

REFERENCES

[1] Martin, Adrien and Thouverez, Fabrice. "Dynamic Analysis and Reduction of a Cyclic Symmetric System Subjected to Geometric Nonlinearities." *Journal of Engineering for Gas Turbines and Power* Vol. 141 (2018). DOI 10.1115/1.4041001.

[2] Seydel, Rüdiger. *Practical Bifurcation and Stability Analysis*, 3rd ed. Interdisciplinary Applied Mathematics, Springer-Verlag, New York (2010).

[3] Fontanela, F., Grolet, A., Salles, L. and Hoffmann, N. "Computation of quasi-periodic localised vibrations in nonlinear cyclic and symmetric structures using harmonic balance methods." *Journal of Sound and Vibration* Vol. 438 (2019): pp. 54–65. DOI 10.1016/j.jsv.2018.09.002.

[4] Detroux, T., Renson, L., Masset, L., Noël, J. P. and Kerschen, G. "Bifurcation Analysis of a Spacecraft Structure Using the Harmonic Balance Method." 2016. American Society of Mechanical Engineers Digital Collection. DOI 10.1115/DETC2015-46259.

[5] Georgiades, F., Peeters, M., Kerschen, G., Golinval, J. C. and Ruzzene, M. "Modal Analysis of a Nonlinear Periodic Structure with Cyclic Symmetry." *AIAA Journal* Vol. 47 No. 4 (2009): pp. 1014–1025. DOI 10.2514/1.40461.

[6] Craig, Roy R. and Bampton, Mervyn C. C. "Coupling of substructures for dynamic analyses." *AIAA Journal* Vol. 6 No. 7 (1968): pp. 1313–1319. DOI 10.2514/3.4741.

[7] MacNeal, R. H. "NASTRAN cyclic symmetry capability. [application to solid rocket propellant grains and space antennas]." 1973.

[8] Castanier, Matthew P. and Pierre, Christophe. "Modeling and analysis of mistuned bladed disk vibration : Status and emerging directions." 2006. DOI 10.2514/1.16345.

[9] Wei, S.-T. and Pierre, C. "Localization Phenomena in Mistuned Assemblies with Cyclic Symmetry Part I: Free Vibrations." *Journal of Vibration, Acoustics, Stress, and Reliability in Design* Vol. 110 No. 4 (1988): pp. 429–438. DOI 10.1115/1.3269547.

[10] Castanier, Matthew P. and Pierre, Christophe. "Using Intentional Mistuning in the Design of Turbomachinery Rotors." *AIAA Journal* Vol. 40 No. 10 (2002): pp. 2077–2086. DOI 10.2514/2.1542.

[11] Martel, Carlos, Corral, Roque and Llorens, José Miguel. "Stability Increase of Aerodynamically Unstable Rotors Using Intentional Mistuning." *Journal of Turbomachinery* Vol. 130 No. 1 (2008). DOI 10.1115/1.2720503.

[12] Biagiotti, Sara, Pinelli, Lorenzo, Poli, Francesco, Vanti, Federico and Pacciani, Roberto. "Numerical Study of Flutter Stabilization in Low Pressure Turbine Rotor with Intentional Mistuning." *Energy Procedia* Vol. 148 (2018): pp. 98–105. DOI 10.1016/j.egypro.2018.08.035.

[13] Lim, Sang-Ho, Bladh, Ronnie, Castanier, Matthew P. and Pierre, Christophe. "Compact, Generalized Component Mode Mistuning Representation for Modeling Bladed Disk Vibration." *AIAA Journal* Vol. 45 No. 9 (2007): pp. 2285–2298. DOI 10.2514/1.13172.

[14] Petrov, E. P. "Analysis of Nonlinear Vibrations Upon Wear-Induced Loss of Friction Dampers in Tuned and Mistuned Bladed Discs." 2013. American Society of Mechanical Engineers Digital Collection. DOI 10.1115/GT2013-95566.

[15] Mitra, Mainak, Zucca, Stefano and Epureanu, Bogdan I. "Adaptive Microslip Projection for Reduction of Frictional and Contact Nonlinearities in Shrouded Blisks." *Journal of Computational and Nonlinear Dynamics* Vol. 11 No. 4 (2016): p. 041016. DOI 10.1115/1.4033003.

[16] Mehrdad Pourkiaee, S. and Zucca, Stefano. "A Reduced Order Model for Nonlinear Dynamics of Mistuned Bladed Disks With Shroud Friction Contacts." *Journal of Engineering for Gas Turbines and Power* Vol. 141 No. 1 (2019): p. 011031. DOI 10.1115/1.4041653.

[17] Mitra, Mainak and Epureanu, Bogdan I. "Dynamic Modeling and Projection-Based Reduction Methods for Bladed Disks With Nonlinear Frictional and Intermittent Contact Interfaces." *Applied Mechanics Reviews* Vol. 71 No. 5 (2019). DOI 10.1115/1.4043083. Publisher: American Society of Mechanical Engineers Digital Collection.

[18] Rosenberg, R. M. "The Normal Modes of Nonlinear n-Degree-of-Freedom Systems." *Journal of Applied Mechanics* Vol. 29 No. 1 (1962): pp. 7–14. DOI 10.1115/1.3636501.

[19] Szemplińska-Stupnicka, W. "The modified single mode method in the investigations of the resonant vibrations of non-linear systems." *Journal of Sound and Vibration* Vol. 63 No. 4 (1979): pp. 475–489. DOI 10.1016/0022-460X(79)90823-X.

[20] Laxalde, Denis and Thouverez, Fabrice. "Complex non-linear modal analysis for mechanical systems: Application to turbomachinery bladings with friction interfaces." *Journal of Sound and Vibration* Vol. 322 No. 4 (2009): pp. 1009–1025. DOI 10.1016/j.jsv.2008.11.044.

[21] Krack, Malte, Panning-von Scheidt, Lars and Wallaschek, Jörg. "A method for nonlinear modal analysis and synthesis: Application to harmonically forced and self-excited mechanical systems." *Journal of Sound and Vibration* Vol. 332 No. 25 (2013): pp. 6798–6814. DOI 10.1016/j.jsv.2013.08.009.

[22] Sombroek, C. S. M., Tiso, P., Renson, L. and Kerschen, G. "Numerical computation of nonlinear normal modes in a modal derivative subspace." *Computers & Structures* Vol. 195 (2018): pp. 34–46. DOI 10.1016/j.compstruc.2017.08.016.

[23] Joannin, Colas, Chouvion, Benjamin, Thouverez, Fabrice, Ousty, Jean-Philippe and Mbaye, Moustapha. "A nonlinear component mode synthesis method for the computation of steady-state vibrations in non-conservative systems." *Mechanical Systems and Signal Processing* Vol. 83 (2017): pp. 75–92. DOI 10.1016/j.ymssp.2016.05.044.

[24] Joannin, Colas, Thouverez, Fabrice and Chouvion, Benjamin. "Reduced-order modelling using nonlinear modes and triple nonlinear modal synthesis." *Computers & Structures* Vol. 203 (2018): pp. 18–33. DOI 10.1016/j.compstruc.2018.05.005.

[25] Nacivet, Samuel, Pierre, Christophe, Thouverez, Fabrice and Jézéquel, Louis. "A dynamic Lagrangian frequency–time method for the vibration of dry-friction-damped systems." *Journal of Sound and Vibration* Vol. 265 No. 1 (2003): pp. 201–219. DOI 10.1016/S0022-460X(02)01447-5.

[26] Muravyov, Alexander A and Rizzi, Stephen A. "Determination of nonlinear stiffness with application to random vibration of geometrically nonlinear structures." *Computers & Structures* Vol. 81 No. 15 (2003): pp. 1513–1523. DOI 10.1016/S0045-7949(03)00145-7.

[27] Kerschen, G., Peeters, M., Golinval, J. C. and Vakakis, A. F. "Nonlinear normal modes, Part I: A useful framework for the structural dynamicist." *Mechanical Systems and Signal Processing* Vol. 23 No. 1 (2009): pp. 170–194. DOI 10.1016/j.ymssp.2008.04.002.

[28] Cameron, T. M. and Griffin, J. H. "An Alternating Frequency/Time Domain Method for Calculating the Steady-State Response of Nonlinear Dynamic Systems." *Journal of Applied Mechanics* Vol. 56 No. 1 (1989): pp. 149–154. DOI 10.1115/1.3176036.

[29] Tran, Duc-Minh. "Component mode synthesis methods using partial interface modes: Application to tuned and mistuned structures with cyclic symmetry." *Computers & Structures* Vol. 87 No. 17 (2009): pp. 1141–1153. DOI 10.1016/j.compstruc.2009.04.009.

[30] Peeters, M., Viguie, R., Serandour, G., Kerschen, G. and Golinval, J.-C. "Nonlinear normal modes, Part II: Toward a practical computation using numerical continuation techniques." *Mechanical Systems and Signal Processing* Vol. 23 No. 1 (2009): pp. 195 – 216. DOI https://doi.org/10.1016/j.ymssp.2008.04.003. Special Issue: Non-linear Structural Dynamics.

[31] Vargiu, P., Firrone, C. M., Zucca, S. and Gola, M. M. "A reduced order model based on sector mistuning for the dynamic analysis of mistuned bladed disks." *International Journal of Mechanical Sciences* Vol. 53 No. 8 (2011): pp. 639–646. DOI 10.1016/j.ijmecsci.2011.05.010.

[32] Corral, Roque, Khemiri, Oualid and Martel, Carlos. "Design of mistuning patterns to control the vibration amplitude of unstable rotor blades." *Aerospace Science and Technology* Vol. 80 (2018): pp. 20–28. DOI 10.1016/j.ast.2018.06.034.

[33] Joannin, C., Chouvion, B., Thouverez, F., Mbaye, M. and Ousty, J.-P. "Nonlinear Modal Analysis of Mistuned Periodic Structures Subjected to Dry Friction." *Journal of Engineering for Gas Turbines and Power* Vol. 138 No. 7 (2016). DOI 10.1115/1.4031886.

[34] Nayfeh, Ali H. and Mook, Dean T. *Nonlinear Oscillations*. John Wiley & Sons (2008).

[35] Quaegebeur, Samuel, Chouvion, Benjamin, Thouverez, Fabrice and Berthe, Loic. "Energy transfer between nodal diameters of cyclic symmetric structures exhibiting polynomial nonlinearities: Cyclic condition and analysis." *Mechanical Systems and Signal Processing* Vol. 139 (2020): p. 106604. DOI 10.1016/j.ymssp.2019.106604.

[36] Thomas, D. L. "Dynamics of rotationally periodic structures." *International Journal for Numerical Methods in Engineering* Vol. 14 No. 1 (1979): pp. 81–102. DOI 10.1002/nme.1620140107.

[37] Monteil, M., Besset, S. and Sinou, J. J. "A double modal synthesis approach for brake squeal prediction." *Mechani-*

cal Systems and Signal Processing Vol. 70-71 (2016): pp. 1073–1084. DOI 10.1016/j.ymssp.2015.07.023.

[38] Sarrouy, Emmanuelle, Grolet, Aurélien and Thouverez, Fabrice. "Global and bifurcation analysis of a structure with cyclic symmetry." *International Journal of Non-Linear Mechanics* Vol. 46 No. 5 (2011): pp. 727–737. DOI 10.1016/j.ijnonlinmec.2011.02.005.

[39] Petrov, E. P. "Analysis of Bifurcations in Multiharmonic Analysis of Nonlinear Forced Vibrations of Gas Turbine Engine Structures With Friction and Gaps." *Journal of Engineering for Gas Turbines and Power* Vol. 138 No. 10 (2016). DOI 10.1115/1.4032906.